Dalton Transactions

Accepted Manuscript

ROYAL SOCIETY OF CHEMISTRY

www.rsc.org/dalton

Journal Name

ARTICLE

High-Pressure and High-Temperature Transformation of Pb(II)-Natrolite to Pb(II)-Lawsonite†

Received 00th January 20xx,
Accepted 00th January 20xx

DOI: 10.1039/x0xx00000x

www.rsc.org/

Junhyuck Im,[a] Yongmoon Lee,[a] Douglas A. Blom,[b] Thomas Vogt[b] and Yongjae Lee*[a]

We report on high-pressure and high-temperature chemical transformations of Pb^{2+}-exchanged natrolite (Pb-NAT, $Pb_8Al_{16}Si_{24}O_{80}{\cdot}16H_2O$) using a combination of in-situ synchrotron X-ray powder diffraction and ex-situ HAADF-STEM real space imaging. Three high-pressure polymorphs of natrolites (Pb-NAT-I, II, III) are observed via step-wise pressure-induced hydrations (PIH) up to 4.5 GPa, during which the number of H_2O molecules located inside the natrolite channel increases from 16 to 40 H_2O per unit cell. At 4.5 GPa after heating the high-pressure Pb-NAT-III phase at 200 ℃ a reconstructive phase transitions into a lawsonite phase (Pb-LAW, $Pb_4Al_8Si_8O_{28}(OH)_8{\cdot}4H_2O$) with orthorhombic space group **P***bnm* and *a*=5.8216(9), *b*=9.114(1) and *c*=13.320(1) Å is observed. The structure of the recovered Pb-LAW phase was characterized using Rietveld refinement of in-situ synchrotron X-ray powder diffraction data and HAADF-STEM real space imaging. In the recovered Pb-LAW phase the Pb^{2+} content is close to 42 wt % and as bond valence approximations reveal Pb^{2+} cations are more tightly coordinated to the framework oxygen atoms than originally in the natrolite phase.

Introduction

The transformation of zeolites into dense minerals under pressure and temperature is of importance for many geophysical and environmental processes.[1] In industrial and environmental remediation processes ion exchange is the first step often followed by densification into a material with better storage properties, lower leaching rates and more efficient recyclability. Studies using Ag-natrolite demonstrated that Cs^+ cations in aqueous solutions can be sequestered in the presence of I^- ions by pressure and temperature and result in the formation of water-free monoclinic pollucite, which is the predominant Cs-containing mineral.[2]

Recycling of printed circuit boards, Pb-based batteries and the anticipated growth of solar energy use requires the adsorption and sequestration of Pb, Cd, Zn and other metals from sometimes quite diluted aqueous waste streams.[3] Natrolite, a small pore zeolite with formula $Na_{16}Al_{16}Si_{24}O_{80}$ x 16 H_2O has an ion exchange capacity of 5.26 meq/g[4] and is an efficient Pb(II) adsorbtive from aqueous solutions as it takes up about 5 mg/g at pH>5.[5] We have investigated the ambient temperature high-pressure chemistry of Pb-natrolite and established the existence of three super-hydrated phases containing 24, 32 and 40 H_2O molecules.[6] In this report we explore the high pressure/high temperature (HP/HT) chemical transformations of Pb-Natrolite ($Pb_8Al_{16}Si_{24}O_{80}$ x 16 H_2O, Pb-NAT) and show that near 4.5 GPa and 200 °C a densification to a Pb-Lawsonite phase ($PbAl_2Si_2O_7(OH)_2$ x H_2O, Pb-LAW) occurs.

Results and discussion

The HP/HT synchrotron X-ray powder diffraction pattern measured up to 4.5(1) GPa using pure water as pressure-transmitting medium (PTM) are shown in Fig. 1. The results show the presence of 6 major phases: (i) the original Pb-NAT ($Pb_8Al_{16}Si_{24}O_{80}$ x 16 H_2O) at ambient pressure and temperature (orthorhombic **F***dd2* space group) and in contact with water (black color), (ii) the first high-pressure super-hydrated monoclinic phase Pb-NAT-I (space group **C***c*, $Pb_8Al_{16}Si_{24}O_{80}$ x 24 H_2O) at 0.4(1) GPa (purple color), (iii) the second

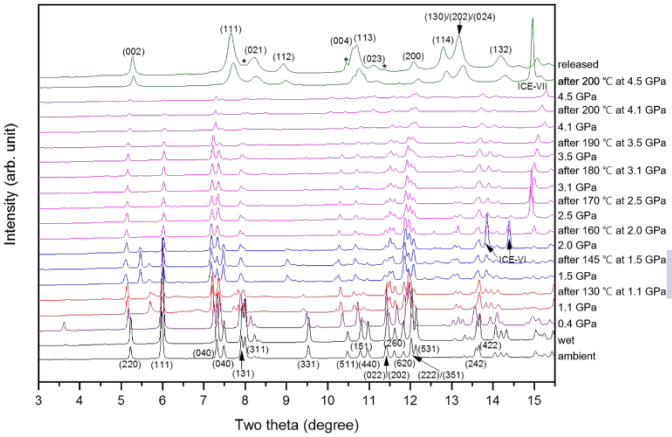

Fig. 1 Pressure- and temperature-induced changes in the synchrotron X-ray powder diffraction patters for Pb-NAT in water pressure medium (PTM). Black line patterns: Pb-NAT, purple line patterns: Pb-NAT-I, red line patterns: Pb-NAT-II, blue line patterns: Pb-NAT-II', magenta line patterns: Pb-NAT-III, olive line patterns: Pb-LAW. Selected Miller indices are shown and the impurity peaks indicate plumbotsumite at released pattern.

[a] *Department of Earth System Sciences, Yonsei University, Seoul 03722, Korea. E-mail: yongjaelee@yonsei.ac.kr*
[b] *NanoCenter & Department of Chemistry and Biochemistry, University of South Carolina, Columbia, SC 29208, USA.*
† Electronic Supplementary Information (ESI) available: Supplementary Figures. See DOI: 10.1039/x0xx00000x

Table 1 Pressure- and temperature-induced changes in the unit-cell parameters and volume. Errors in pressure and temperature measurements are estimated to be ±0.1 GPa and ±10 °C, respectively.

P (GPa)	treatment	phase	space group	a (Å)	b (Å)	c (Å)	α (°)	β (°)	γ (°)	V (Å³)
0.0	ambient	Pb-NAT	**F***dd2*	18.8220(5)	19.2673(5)	6.5373(2)	90.000	90.000	90.000	2370.8(1)
0.0	wet	Pb-NAT	**F***dd2*	18.8325(4)	19.2605(4)	6.5272(2)	90.000	90.000	90.000	2367.6(1)
0.4		Pb-NAT-I	**C***c*	6.5170(2)	19.4617(6)	10.1122(3)	90.000	109.351(2)	90.000	1210.10(8)
1.1		Pb-NAT-II	**C***c*	6.4835(3)	19.1502(10)	10.3406(5)	90.000	109.012(3)	90.000	1213.9(1)
	130 °C, 1 h	Pb-NAT-II	**C***c*							
1.5		Pb-NAT-II′	**C***1*	19.697(1)	19.328(1)	6.4715(4)	90.179(5)	90.147(5)	89.713(4)	2463.7(4)
	145 °C, 1 h	Pb-NAT-II′	**C***1*							
2.0		Pb-NAT-II′	**C***1*	19.6666(8)	19.2765(9)	6.4739(2)	90.110(2)	90.037(3)	89.765(2)	2454.3(3)
	160 °C, 1 h	Pb-NAT-III	**F***dd2*							
2.5		Pb-NAT-III	**F***dd2*	19.184(1)	19.5912(9)	6.4592(3)	90.000	90.000	90.000	2427.6(3)
	170 °C, 1 h	Pb-NAT-III	**F***dd2*							
3.1		Pb-NAT-III	**F***dd2*	19.146(1)	19.555(1)	6.4547(4)	90.000	90.000	90.000	2416.6(4)
	180 °C, 1 h	Pb-NAT-III	**F***dd2*							
3.5		Pb-NAT-III	**F***dd2*	19.122(2)	19.518(1)	6.4526(5)	90.000	90.000	90.000	2408.3(5)
	190 °C, 1 h	Pb-NAT-III	**F***dd2*							
4.1		Pb-NAT-III	**F***dd2*	19.005(2)	19.442(3)	6.468(1)	90.000	90.000	90.000	2389.9(8)
	200 °C, 1 h	Pb-NAT-III	**F***dd2*							
4.5		Pb-NAT-III	**F***dd2*	19.006(4)	19.407(4)	6.467(1)	90.000	90.000	90.000	2385(1)
4.5	200 °C, 9 h	Pb-LAW	**P***bnm*	5.7834(8)	8.982(2)	13.265(2)	90.000	90.000	90.000	689.1(2)
0.00	released	Pb-LAW	**P***bnm*	5.8216(9)	9.114(1)	13.320(1)	90.000	90.000	90.000	706.8(2)

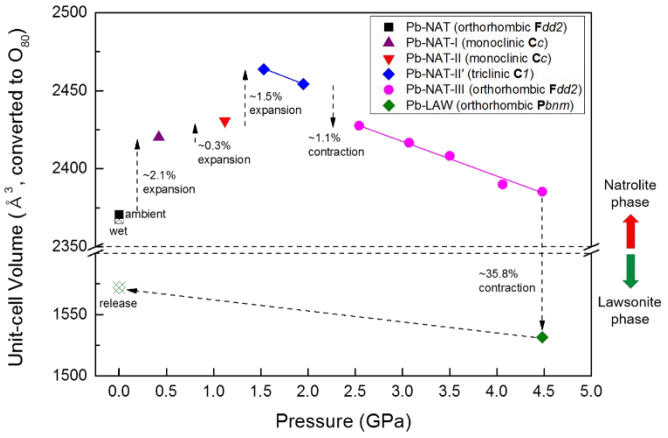

Fig. 2 Changes of the unit-cell volume as a function of pressure and temperature. The unit-cell volume is normalized to 80 framework oxygen atoms from Pb-NAT-I, II and Pb-LAW to comparison with other high-pressure phases of Pb-NAT in water pressure medium.

super-hydrated monoclinic phase Pb-NAT-II (space group **C***c*, $Pb_8Al_{16}Si_{24}O_{80}$ x 32 H_2O) near 1.1(1) GPa and 130 °C (red color), (iv) a transient **C***1* triclinic phase Pb-NAT-II′ between 1.5(1) and 2.0(1) GPa and 145 °C (blue color), (v) the third high-pressure orthorhombic phase Pb-NAT-III ($Pb_8Al_{16}Si_{24}O_{80}$ x 40 H_2O) with space group **F***dd2* between 2.0(1) GPa and 4.5(1) GPa and temperatures up to 200 °C (magenta colour), and (vi) a densified phase obtained after 9 hours of heating at 200 °C and 4.5 GPa which is recovered after pressure release at ambient temperature.

As Pb-NAT is pressurized in water, pressure-induced hydration (PIH) occurs in two steps to form two monoclinic phases Pb-NAT-I and Pb-NAT-II both with space group **C***c* space. Above 1.5(1) GPa and heating at 145 °C for 1 hour, several peaks including the (220), (111) show notable broadening and splitting (Fig. S1). A Pb-NAT-II′ phase can be indexed in the triclinic space group **C***1* which has not been observed in our previous study done without heating the sample (Fig. S2)[6]. Transition from Pb-NAT-II′ to Pb-NAT-III occurs with a concomitant volume contraction at 2.0(1) GPa after heating at various temperatures for 1 hour (see table 1). The symmetry space group reverts back to orthorhombic with space group **F***dd2*. The Pb-NAT-III phase is present up to 4.5(1) GPa with intermittent heating for periods of 1 hour (see table 1). The HP and HP/HT process up to 4.5(1) GPa differs in the presence of the Pb-NAT-II″ phase in the latter.

Subsequent heating at 200 °C for 9 hours at 4.5(1) GPa completely transforms Pb-NAT-III into a dense phase with a ca. 36% smaller unit cell volume and a new orthorhombic space group **P***bnm*. This material can be recovered from the gasket of the pressure cell after pressure release.

Changes of the unit cell volume of the various super-hydrated phases under pressure and pressure/temperature conditions are shown in Fig. 2 (also see Table 1). At 0.4(1) GPa Pb-NAT transforms

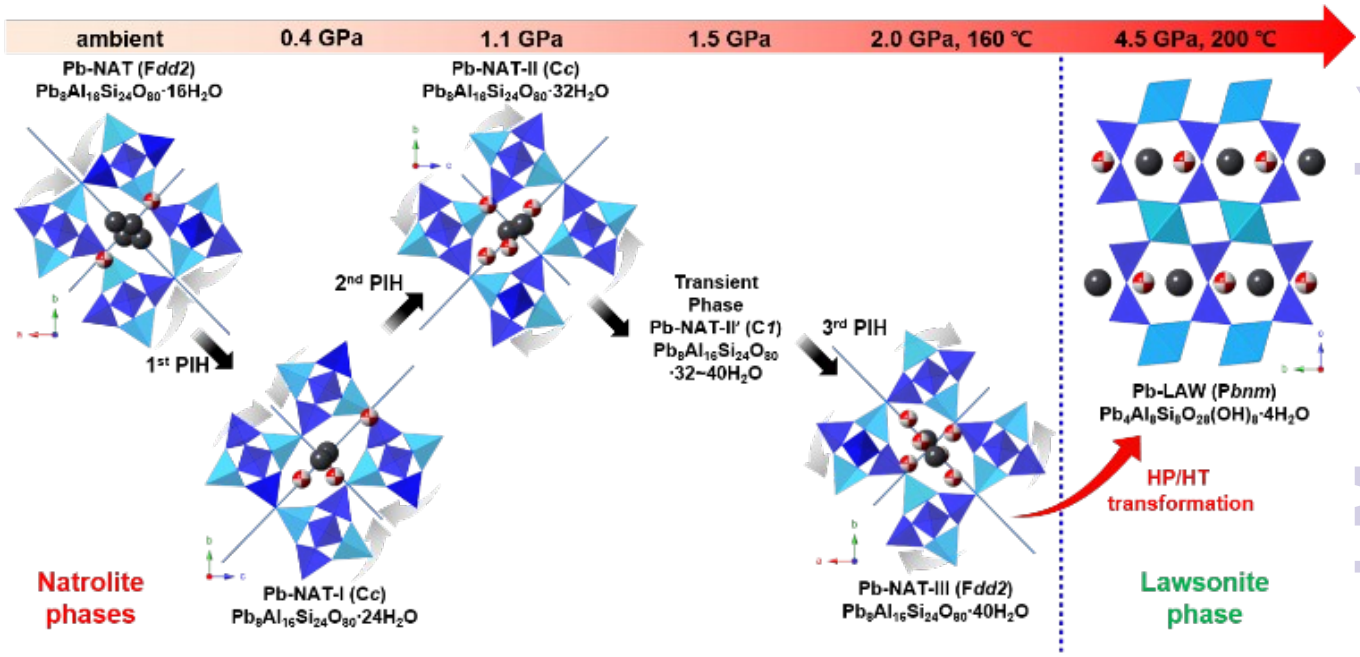

Fig. 3 Polyhedral representations of the pressure- and temperature-driven transformations of Pb-NAT in the presence of water. Two-toned polyhedral in the natrolite and lawsonite framework illustrate the ordered arrangements of the Si-, Al-O_4 tetrahedra , SiO_4 tetrahedra and AlO_6 octahedra, respectively. Dark grey ball: Pb^{2+}, red-grey two toned ball: oxygen for H_2O molecules.

Table 2 Refined atomic coordinates for Pb-NAT with pure water Pressure-Transmitting Medium (PTM) as a function of pressure.[a]

Pressure (GPa)		0.4			1.1			2.5			released
Phase		Pb-NAT-I			Pb-NAT-II			Pb-NAT-III			Pb-LAW
Space group		**C***c*			**C***c*			**F***dd2*			**P***bnm*
Unit-cell composition (80 framework oxygen)		$Pb_8Al_{16}Si_{24}O_{80}$·($24H_2O$)			$Pb_8Al_{16}Si_{24}O_{80}$·($32H_2O$)			$Pb_8Al_{16}Si_{24}O_{80}$·($40H_2O$)			$Pb_4Al_8Si_8O_{28}$ $(OH)_8$·$4(H_2O)$
wRp(%), χ2		3.65, 2.951			2.69, 3.716			2.25, 1.081			1.79, 4.456
Si1 4a	*x*	0.5632(11)	Si1 4a	*x*	0.6028(14)	Si1 8a	*x*	0.00	Si1 8d	*x*	-0.0002(17)
	y	0.3723(4)		*y*	0.3750(4)		*y*	0.00		*y*	-0.0042(9)
	z	-0.0521(10)		*z*	-0.0732(12)		*z*	0.00		*z*	0.87153(21)
	U_{iso}	0.005(4)		U_{iso}	0.046(5)		U_{iso}	0.002(4)		U_{iso}	0.068(11)
Si2 4a	*x*	0.2411(12)	Si2 4a	*x*	0.2802(14)	Si2 16b	*x*	0.16092(29)	Al1 8d	*x*	0.2499(19)
	y	0.28547(33)		*y*	0.28485(31)		*y*	0.20696(21)		*y*	0.2500(6)
	z	0.0337(8)		*z*	0.0161(9)		*z*	0.6167(6)		*z*	0.0000(4)
Si3 4a	*x*	0.6407(12)	Si3 4a	*x*	0.6944(14)	Al1 16b	*x*	0.04421(23)			
	y	0.03640(35)		*y*	0.03341(29)		*y*	0.08564(29)	O1 4c	*x*	0.000(4)
	z	0.3484(9)		*z*	0.3479(8)		*z*	0.6096(5)		*y*	0.0186(21)
Al1 4a	*x*	0.0435(12)	Al1 4a	*x*	1.0868(14)					*z*	0.25
	y	0.4184(4)		*y*	0.41827(27)	O1 16b	*x*	0.0126(4)		U_{iso}	0.052(11)
	z	0.1229(8)		*z*	0.1060(9)		*y*	0.06679(12)	O2 8d	*x*	0.7250(20)
Al2 4a	*x*	0.3588(12)	Al2 4a	*x*	0.4033(14)		*z*	0.8572(6)		*y*	0.4127(16)
	y	0.16634(33)		*y*	0.16821(30)		U_{iso}	0.017(6)		*z*	0.4076(13)
	z	0.2593(8)		*z*	0.2561(9)	O2 16b	*x*	0.0894(4)	O3 8d	*x*	0.0001(17)
							y	0.1632(4)		*y*	0.8339(15)
O1 4a	*x*	0.5983(31)	O1 4a	*x*	0.6153(31)		*z*	0.6069(10)		*z*	0.9231(8)
	y	0.0301(6)		*y*	0.0249(5)	O3 16b	*x*	0.0988(4)	O4 8d	*x*	-0.0002(22)
	z	0.4969(13)		*z*	0.4804(15)		*y*	0.0192(5)		*y*	0.3470(12)
	U_{iso}	0.020(6)		U_{iso}	0.046(6)		*z*	0.5291(12)		*z*	0.9311(8)
O2 4a	*x*	0.6376(19)	O2 4a	*x*	0.6613(23)	O4 16b	*x*	0.2233(5)	O5 8d	*x*	0.2746(20)
	y	-0.0402(4)		*y*	-0.0396(4)		*y*	0.15688(34)		*y*	0.4128(16)
	z	0.2853(9)		*z*	0.2647(10)		*z*	0.6906(12)		*z*	0.0924(13)
O3 4a	*x*	0.4581(22)	O3 4a	*x*	0.5544(21)	O5 16b	*x*	0.18163(13)			
	y	0.0847(4)		*y*	0.0937(5)		*y*	0.2378(4)	Pb1 4c	*x*	-0.0231(25)
	z	0.2410(13)		*z*	0.2473(13)		*z*	0.3923(6)		*y*	0.3433(9)

O4 4a	*x*	0.1424(20)	O4 4a	*x*	0.1690(19)					*z*	0.25
	y	0.1586(8)		*y*	0.1422(6)	Pb1 16b	*x*	0.2351(4)		*Occu.*	1.00
	z	0.3243(14)		*z*	0.2920(13)		*y*	0.02780(30)		U_{iso}	0.128(5)
O5 4a	*x*	0.2674(23)	O5 4a	*x*	0.3341(25)		*z*	0.5836(25)			
	y	0.20842(35)		*y*	0.2117(4)		*Occu.*	0.50	OW1 4c	*x*	0.099(16)
	z	0.0974(8)		*z*	0.0988(11)		U_{iso}	0.0758(33)		*y*	0.624(12)
O6 4a	*x*	0.0616(20)	O6 4a	*x*	0.0579(18)					*z*	0.25
	y	0.2844(6)		*y*	0.2769(5)	OW1 16b	*x*	0.4466(18)		*Occu.*	1.00
	z	-0.1218(10)		*z*	-0.1126(15)		*y*	0.1729(21)		U_{iso}	0.128(5)
O7 4a	*x*	0.4694(17)	O7 4a	*x*	0.4765(22)		*z*	0.455(6)			
	y	0.3105(7)		*y*	0.3072(7)		*Occu.*	1.00			
	z	0.0187(16)		*z*	-0.0401(13)		U_{iso}	0.0758(33)			
O8 4a	*x*	0.1704(24)	O8 4a	*x*	0.2545(21)	OW2 16b	*x*	0.1003(24)			
	y	0.3384(5)		*y*	0.3452(5)		*y*	0.1505(21)			
	z	0.1343(13)		*z*	0.1195(13)		*z*	0.138(7)			
O9 4a	*x*	0.8781(16)	O9 4a	*x*	0.9487(16)		*Occu.*	1.00			
	y	0.0707(7)		*y*	0.0564(6)	OW3 16b	*x*	0.047(4)			
	z	0.3775(18)		*z*	0.3981(16)		*y*	0.2654(24)			
O10 4a	*x*	0.7616(13)	O10 4a	*x*	0.8157(14)		*z*	0.093(27)			
	y	0.4073(8)		*y*	0.3900(6)		*Occu.*	0.50			
	z	0.0710(15)		*z*	0.0588(15)						
Pb1 4a	*x*	0.3714(17)	Pb1 4a	*x*	0.4874(26)						
	y	0.09861(23)		*y*	0.1082(5)						
	z	0.9648(10)		*z*	-0.0226(13)						
	Occu.	0.889(4)		*Occu.*	0.524(5)						
	U_{iso}	0.0389(13)		U_{iso}	0.0530(18)						
Pb2 4a	*x*	0.460(4)	Pb2 4a	*x*	0.5448(28)						
	y	0.3777(17)		*y*	0.3674(5)						
	z	0.4211(33)		*z*	0.3824(14)						
	Occu.	0.111(4)		*Occu.*	0.476(5)						
OW1 4a	*x*	0.812(7)	OW1 4a	*x*	0.877(7)						
	y	0.3094(21)		*y*	0.2708(25)						
	z	0.282(4)		*z*	0.212(4)						
	Occu.	1.00		*Occu.*	1.00						
	U_{iso}	0.037(12)		U_{iso}	0.029(10)						
OW2 4a	*x*	0.654(5)	OW2 4a	*x*	0.660(9)						
	y	0.4754(19)		*y*	0.4585(28)						
	z	0.2617(35)		*z*	0.244(5)						
	Occu.	1.00		*Occu.*	1.00						
OW3 4a	*x*	0.196(7)	OW3 4a	*x*	0.213(4)						
	y	0.6824(19)		*y*	0.6899(10)						
	z	0.018(4)		*z*	-0.103(4)						
	Occu.	1.00		*Occu.*	1.00						
			OW4 4a	*x*	-0.005(9)						
				y	0.0560(27)						
				z	0.054(5)						
				Occu.	1.00						

Table 3 Selected bond distances (Å) and angles(°) within the framework and non-framework atoms for Pb-NAT with pure water Pressure-Transmitting Medium (PTM) as a function of pressure (less than 3.00 Å).[a]

Pressure (GPa)		0.4		1.1		2.5		released
Phase		Pb-NAT-I		Pb-NAT-II		Pb-NAT-III		Pb-LAW
Framework	Si1-O4	1.6188(17)	Si1-O4	1.6200(13)	Si1-O1 x2	1.6194(10)	Si1-O1	1.6244(23)
	Si1-O7	1.6200(17)	Si1-O7	1.629(6)	Si1-O5 x2	1.6194(10)	Si1-O2	1.6248(21)
	Si1-O9	1.6200(17)	Si1-O9	1.6197(13)			Si1-O3	1.6242(21)
	Si1-10	1.6192(17)	Si1-10	1.6199(13)	Si2-O2	1.6191(10)	Si1-O5	1.6247(21)
					Si2-O3	1.6200(10)		

	Si2-O5	1.6193(17)	Si2-O5	1.6195(12)	Si2-O4	1.6197(10)	Al1-O2	1.9295(22)
	Si2-O6	1.6199(12)	Si2-O6	1.6198(12)	Si2-O5	1.6194(10)	Al1-O3	1.9361(21)
	Si2-O7	1.6200(17)	Si2-O7	1.6198(12)			Al1-O3	1.9361(21)
	Si2-O8	1.6192(17)	Si2-O8	1.6198(12)	Al1-O1	1.7492(10)	Al1-O4	1.9334(22)
					Al1-O2	1.7492(10)	Al1-O4	1.9335(22)
	Si3-O1	1.6199(17)	Si3-O1	1.6198(12)	Al1-O3	1.7496(10)	Al1-O5	1.9293(22)
	Si3-O2	1.6193(17)	Si3-O2	1.6198(17)	Al1-O4	1.7499(10)		
	Si3-O3	1.6196(17)	Si3-O3	1.6195(12)			O1-SI1-O2	109.7(6)
	Si3-O9	1.6205(17)	Si3-O9	1.6199(12)	Si1-O1-Al1	138.00(32)	O1-SI1-O3	110.4(5)
					Si2-O2-Al1	151.6(5)	O1-SI1-O5	109.6(6)
	Al1-O1	1.7496(17)	Al1-O1	1.7498(12)	Si2-O3-Al1	133.1(4)	O2-SI1-O3	109.8(6)
	Al1-O2	1.7483(17)	Al1-O2	1.7494(12)	Si2-O4-Al1	135.0(4)	O2-SI1-O5	107.6(4)
	Al1-O8	1.7489(17)	Al1-O8	1.7497(12)	Si1-O5-Si2	139.6(4)	O3-SI1-O5	109.8(6)
	Al1-10	1.7494(17)	Al1-10	1.7494(17)				
							O2-Al1-O3	91.15(33)
	Al2-O3	1.7496(17)	Al2-O3	1.7505(12)			O2-Al1-O3	88.85(33)
	Al2-O4	1.7493(17)	Al2-O4	1.7507(12)			O2-Al1-O4	89.4(4)
	Al2-O5	1.7492(17)	Al2-O5	1.7492(17)			O2-Al1-O4	90.6(4)
	Al2-O6	1.7492(17)	Al2-O6	1.7492(17)			O3-Al1-O4	97.8(4)
							O3-Al1-O4	82.26(10)
	Si3-O1-Al1	140.4(6)	Si3-O1-Al1	134.8(5)			O3-Al1-O5	88.86(33)
	Si3-O2-Al1	138.6(5)	Si3-O2-Al1	147.7(5)			O3-Al1-O4	82.26(10)
	Si3-O3-Al2	132.2(6)	Si3-O3-Al2	138.9(7)			O3-Al1-O4	97.72(35)
	Si1-O4-Al2	145.7(8)	Si1-O4-Al2	137.0(7)			O3-Al1-O5	91.15(33)
	Si2-O5-Al2	139.9(5)	Si2-O5-Al2	148.0(6)			O4-Al1-O5	90.6(4)
	Si2-O6-Al2	143.0(6)	Si2-O6-Al2	135.5(6)			O4-Al1-O5	89.4(4)
	Si1-O7-Si2	139.2(8)	Si1-O7-Si2	142.5(9)				
	Si2-O8-Al1	138.7(7)	Si2-O8-Al1	135.5(6)			SI1-O1-SI1	170.8(17)
	Si1-O9-Si3	152.8(9)	Si1-O9-Si3	141.4(8)				
	Si1-O10-Al1	140.7(8)	Si1-O10-Al1	142.5(8)				
Non-Framework	Pb1-O1	2.872(15)	Pb1-O1	2.678(14)	Pb1-O2	2.926(14)	Pb1-O2	2.909(15)
	Pb1-O3	2.674(16)	Pb1-O3	2.696(18)	Pb1-O3	2.692(9)	Pb1-O3	2.642(10)
	Pb1-O5	2.726(11)	Pb1-O5	2.702(16)	Pb1-O4	2.590(9)	Pb1-O4	2.632(9)
	Pb1-Pb2	2.608(28)	Pb1-Pb2	2.754(12)	Pb1-OW1	2.426(10)	Pb1-OW1	2.73(4)
	Pb1-OW1	2.51(4)	Pb1-OW2	2.94(6)		2.502(27)	Pb1-OW1	2.56(5)
	Pb1-OW2	2.526(16)	Pb1-OW2	2.464(12)	Pb1-OW2	2.87(4)	Pb1-OW2	2.91(5)
	Pb1-OW3	2.58(4)			Pb1-OW3	2.412(10)	Pb1-OW3[b]	2.14(14)
			Pb2-O2	2.978(21)		2.404(10)	Pb1-OW3[b]	1.80(16)
	Pb2-O2	2.638(29)	Pb2-O5	2.844(25)				
	Pb2-O5	2.762(31)	Pb2-O6	2.766(14)	OW1-O1	2.559(10)	OW1-O1	2.515(32)
	Pb2-O8	2.99(4)	Pb2-O8	2.790(23)	OW1-OW2	2.587(10)	OW1-OW2	2.38(4)
	Pb2-OW3	2.537(16)	Pb2-OW2	2.52(5)		2.956(18)	OW1-OW3	2.80(9)
			Pb2-OW3	2.463(12)	OW1-OW3	2.580(10)	OW1-OW3	2.64(15)
.	OW1-O6	2.83(5)	Pb2-OW4	2.40(5)				
	OW1-O7	2.86(4)			OW2-O1	2.87(4)	OW2-O1	2.97(4)
	OW1-O10	2.80(5)	OW1-OW3	2.502(13)	OW2-O5	2.95(4)	OW2-O5	2.84(4)
	OW1-OW3	2.83(5)			OW2-OW3	2.53(4)	OW2-OW3	2.488(10)
			OW2-OW4	2.67(5)				
	OW2-O3	2.96(4)			OW3-O3	2.659(18)	OW3-O2	2.98(6)
	OW2-O10	2.62(5)			OW3-O5	2.618(16)	OW3-O3	2.84(14)
							OW3-O4	2.97(6)
	OW3-O7	2.90(4)						

[a] ESD's are in parentheses. Restraints on the Si, Al-O and O-O bond distances have been applied (see Experimental Methods).

[b] Pb1-OW3 distance is about 2 Å cause that simultaneous occupancy is excluded.

to Pb-NAT-I and the unit-cell volume expands by ca. 2.1 % due to the insertion of 8 additional H_2O molecules to form $Pb_8Al_{16}Si_{24}O_{80}{\cdot}24H_2O$. After further pressure increase and short heating for 1 hour, a second unit-cell volume expansion by ca. 0.3 % is observed near 1.5(1) GPa and related to a second pressure-induced hydration forming Pb-NAT-II with 8 more H_2O molecules inside the natrolite channel ($Pb_8Al_{16}Si_{24}O_{80}{\cdot}32H_2O$). Further increase in pressure to 2.0(1) GPa and intermittent heating for 1 hour periods then results in the formation of a new phase Pb-NAT-II' which is indexed as triclinic with space group **C***1* (see Fig. S2). This triclinic phase has not been observed yet in the Pb-natrolite system but observed in other divalent cation exchanged natrolites, such as Ca-NAT and Sr-NAT.[6] Heating at 2.0(1) GPa leads to the formation of Pb-NAT-III ($Pb_8Al_{16}Si_{24}O_{80}{\cdot}40H_2O$) which gradually contracts up to 4.5(1) GPa. After 9 hours of heating at 200 °C and 4.5(1) GPa, a significant densification occurs and the unit-cell volume contracts by ca. 36 %. This dense phase is identified as Pb(II)-lawsonite ($PbAl_2Si_2O_7(OH)_2{\cdot}H_2O$, Pb-LAW). After pressure release, small traces of plumbotsumite ($Pb_5Si_4O_8(OH)_{10}$) are also found and indicated by asterisks in Fig. 1.

An overview of the pressure- and temperature-induced phase transformations of Pb-NAT is depicted in Fig. 3. The structural models of Pb-NAT-I, Pb-NAT-II, Pb-NAT-III and Pb-LAW were confirmed by Rietveld refinements (Table 2, 3 and Fig. S3).[6-9] The structure of Pb-NAT at ambient condition was taken from Lee (2010).[9] The initial atom coordinates of Pb-NAT-I, Pb-NAT-II and Pb-NAT-III were determined by Seoung (2015).[6] The original Pb-NAT has two different Pb^{2+} cation sites which are statistically occupied in the natrolite channels. The structure of Pb-NAT-I near 0.4(1) GPa is similar to the reported Na-paranatrolite phase with 24 H_2O per 80 framework oxygen atoms.[10, 11] In Pb-NAT-I the statistical occupation of the Pb^{2+} cations is maintained and symmetry changes are due to the inversion of the major and minor axes of the elliptical channels. The second PIH at 1.1(1) GPa leads to the Pb-NAT-II phase with 32 H_2O per 80 framework oxygen atoms while maintaining the cation disorder, symmetry and orientation of the major and minor axes. At 1.5(1) GPa and 130 °C heating for 1 hour a triclinic Pb-NAT-II' phase is observed. This phase is expected to continuously increase the H_2O molecule content from 32 to 40 per 80 framework oxygen atoms. Between 2.0(1) and 4.5(1) GPa and heating up to 200 °C, the third PIH forms the orthorhombic phase Pb-NAT-III where the major and minor axes are reverted back to the original orientation they had in Pb-NAT (see Fig. 3).

After 9 hours of heating at 200 °C and 4.5 GPa, Pb-NAT-III completely transforms to Pb-LAW. Pb-LAW ($PbAl_2Si_2O_7(OH)_2{\cdot}H_2O$) has a new framework made up of edge-sharing $AlO_{6/2}$ octahedral chains running parallel to the *a*-axis which are linked by Si_2O_7 groups and H_2O molecules. In comparison to $CaAl_2Si_2O_7(OH)_2{\cdot}H_2O$ (Ca-LAW) with space group **C***mcm*, Pb-LAW crystallizes in the 'klassengleiche' subgroup **P***bnm* as a result of its stereo-chemically active $6s^2$ lone pair.[8] The structure of Pb-LAW has only one atomic site for the Pb^{2+} cations and 4 H_2O molecules are located inside the lawsonite channels. Both cation sites and oxygen sites of H_2O refine to full occupation.

In order to characterize the structure of the recovered material, we initially used High-Angle Annular Dark Field Scanning Transmission Electron Microscope (HAADF-STEM) real-space imaging (Fig. 4a). The strong Z contrast peaks observed in the HAADF-STEM images are due to regular interatomic Pb-Pb spacings of ca. 6.7 Å along the *c*-axis (Fig. 4b). The Pb-Pb distance along the *c*-axis was later determined to 6.66(2) Å by Rietveld refinement (Fig. 4c). The reconstructive nature of the Pb-NAT-III to Pb-LAW phase transition can also be see in scanning electron microscopy (SEM) images which reveal very different morphologies (Fig. 4d).

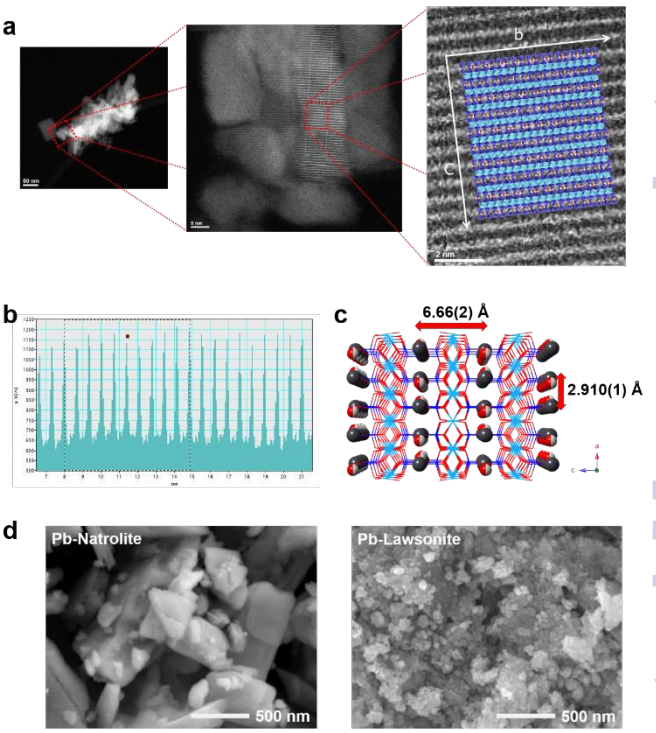

Fig. 4 (a) HAADF-STEM images from a recovered Pb-LAW particle viewed do wn [100]. The crystal structure of the refined Pb-LAW is overlaid on the exp erimental HAADF-STEM image to show the Z-contrast matching the distribut ion of the Pb^{2+} extra-framework cations in the model. (b) Contrast indicating the Pb-Pb distances along the c-axis (c) Refined Pb-Pb distance in the struct ure of Pb-LAW along *a*-axis and *c*-axis. (d) SEM images of the morphology of Pb-NAT (left) and the recovered Pb-LAW (right) after pressure release.

We propose that the transition from Pb-NAT-III to Pb-LAW is facilitated by the migration of Pb^{2+} to a more stable environment under HP/HT conditions. The two atomic sites of Pb^{2+} in Pb-NAT at ambient conditions are coordinated to 4 oxygen atoms from the framework and H_2O molecules, whereas the Pb^{2+} cations in Pb-LAW are coordinated by 8 oxygen atoms from the framework and H_2O molecules (Fig. 5a) resulting in a more favourable environment as corroborated by simple Bond Valence Sum (BVS) calculations (Fig. 5b). The BVS for the Pb^{2+} atoms in Pb-NAT, Pb-NAT-I, Pb-NAT-II, Pb-NAT-III and Pb-LAW are calculated to as 1.58, 1.43, 1.60, 2.19 and 1.89, respectively. These variations are larger than any variations due to using ambient pressure and temperature d_0 values and indicates a significant under-bonding of Pb^{2+} in Pb-NAT, PbNAT-I and Pb-NAT-II whereas in Pb-NAT-III and Pb-LAW the BVS is closer to the formal valence of 2.[12]

To establish the presence of hydroxyl groups and further confirm our structural model we measured the FTIR spectra and noted the presence of distinct vibrational modes for Pb-LAW[13-15] and Pb-NAT[16-18] (Fig. 5c). Clearly visible are vibrational modes due to the different

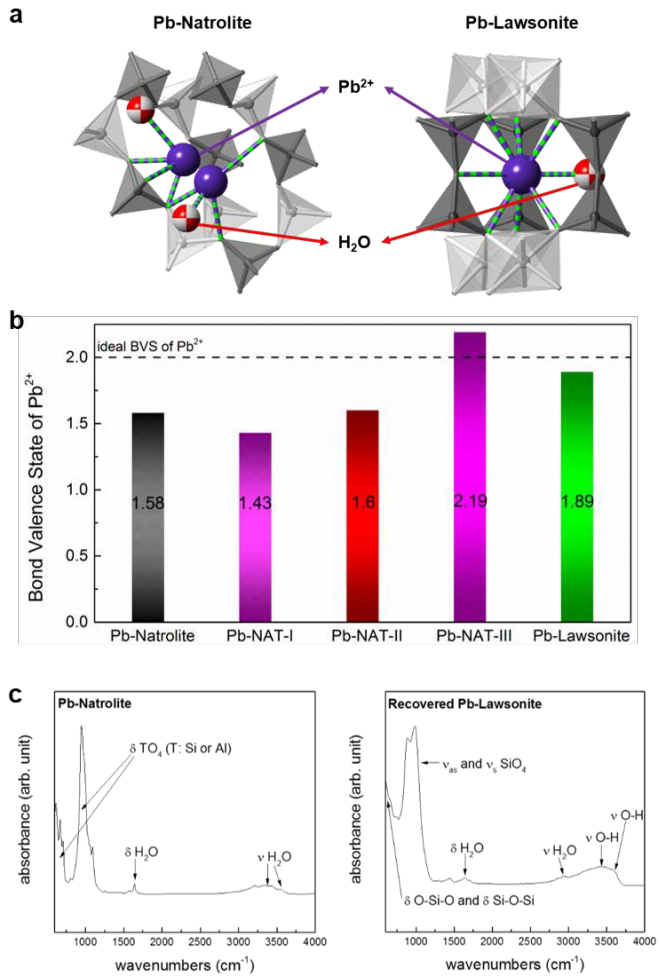

Fig. 5. (a) Coordination of Pb^{2+} cations in (left) Pb-NAT and (right) the recovered Pb-LAW. (b) Bond valence sum (BVS) comparison for Pb^{2+} in the starting sample (Pb-NAT), high pressure phases (Pb-NAT-I, II, III) and recovered sample (Pb-LAW). Ideal BVS of Pb is 2. (c) FTIR powder spectra (600 ~ 4000 cm^{-1}) of (left) Pb-Natrolite and (right) the recovered Pb-Lawsonite showing H_2O, OH, SiO_4, AlO_4 and Si_2O_7 regions.

framework topology (T=Al,Si) as well as enhanced modes near 3500 cm^{-1}, indicative of the hydroxyl groups.

Conclusions

In conclusion, we have shown that high pressure- and high temperature-driven chemical transformations of lead cation exchanged natrolite (Pb-NAT) in the pressure and temperature range up to 4.5 GPa and 200 ℃ result in 4 successive pressure-induced hydrations and one reconstructive phase transformation. The latter densification of small pore natrolites to a dense lawsonite phase results in an enrichment of lead to nearly 42 wt. % Pb^{2+}. Our results suggest that these processes might have the potential to remediate, store and recycle environmentally-harmful lead.

Experimental

Sample powder preparation

The preparation methods for Pb-exchanged natrolite (labeled Pb-NAT) were described in details by Lee *et al.*[9, 19, 20] Before making Pb-NAT, K-exchanged natrolite (K-NAT) was prepared using a 4 M KNO_3 (ACS reagent grade from Sigma-Aldrich) solution and a ground natural natrolite mineral (ideally $Na_{16}Al_{16}Si_{24}O_{80}16H_2O$, San Juan, Argentina, from OBG International) in a 100:1 weight ratio. The solid in solution was stirred at 80 °C and the loss of water was minimized in a closed system. After 24 hours, the solid was separated from the solution using a centrifuge and the dried powder was used for a second and third exchange step under the same conditions. The final product was air-dried, and based on the elemental analysis (Jarrell-Ash Polyscan 61E Inductively Coupled Plasma) an over 99% K-exchange was confirmed. After K-exchange, further cation-exchange was done using a similar solution-exchange process by stirring a mixture of powdered K-NAT and a 1 M $PbNO_3$ in a 100:1 weight ratio in a closed system at 80 °C for 24 hours. Three total exchange steps were done, and a nearly fully Pb- exchange was confirmed, qualitatively, using Electron Probe Micro Analysis (EPMA) method which indicated that the residual potassium ions could only be detected at amounts < 0.1%.

Synchrotron X-ray diffraction

In-situ high-pressure synchrotron X-ray diffraction on Pb-NAT were conducted at beamline 9A at the Pohang Accelerator Laboratory (PAL) in Korea. The X-rays coming from the in-vacuum undulator (IVU) are monochromatized using a Si (111) double crystal setup and focused at the detector position using Kirkpatrick-Baez-type mirrors. The X-ray energy used is 20.14 keV (0.6155(1) Å). X-ray diffraction patterns were recorded with a 2D CCD detector (Rayonix SX165) and the acquisition time was ca. 10 - 30 seconds dependent on the saturation of the detector. The Fit2D program was use to convert 2D diffraction data to 1D ones with azimuthal integration.[21] Diffraction angles were calibrated using a standard sucrose (Monoclinic, a = 10.8631 Å, b = 8.7044 Å, c = 7.7624 Å, β = 102.938°) and the wavelength of the incident beam was determined using a LaB_6 standard reference material (SRM 660b, a = 4.15692(1) Å).

High-pressure experiments

A modified Merrill-Bassett type diamond anvil cell (DAC) with two opposed diamond anvil supported by tungsten-carbide plates[22] was used for the high-pressure experiments. The anvils used were brilliant-cut type-1A diamonds with a culet diameter of 600 µm. The DAC has a rectangular asymmetric slot on one side to provide an opening of ca. 40 degrees, through which diffraction data are measured. The powdered Pb-NAT sample was loaded into a 300 µm diameter with a 130 µm thick sample chamber obtained by electro-spark erosion in a pre-indented stainless steel foil gasket. A few ruby spheres of ~20 µm diameter were added as a pressure gauge. Subsequently, the distilled pure water was added to the sample chamber as a hydrostatic pressure-transmitting medium (PTM).[23] The pressure at the sample in the DAC was measured by detecting the shift of R1 emission line of the included ruby spheres (precision: ±0.05 GPa).[24] The pressure was calculated using the equation below (1) :

$$P = A/B\{[1 + (\Delta\lambda/\lambda_0]^B - 1\} \quad (1)$$

where P is the pressure in megabars, λ is the wavelength of the ruby R line, A = 19.04 Mbar, B = 7.665.[25] The sample was equilibrated for about 10 to 15 minutes in the DAC at each adjusted pressure. After collecting the XRD data, the DAC was occasionally heat-treated in an oven at 130 °C up to 200 °C. All the heating treatments were for an hour except for the last heating step of 9 hours at 200 °C (Fig. 1). Pressure dependent changes of the unit-cell parameters and volumes (Table 1) were derived from a series of whole profile fitting procedure using the GSAS suite of programs.[26]

Crystal structure refinement

The structural models of the high-pressure phases were characterized using Rietveld refinement methods.[27] The background was fitted with a Chebyshev polynomial with up to 30 coefficients, and the pseudo-Voigt profile function was used to fit the observed Bragg diffraction peaks. In order to reduce the number of variables, isotropic displacement factors were refined by grouping the framework tetrahedral atoms, framework oxygen atoms, and non-framework cations and water oxygen atoms, respectively. For the high-pressure models, all the isotropic displacement factors were grouped to be the same. Geometrical soft-restraints on the T-O (T = Si, Al) and O-O bond distances of the tetrahedra and the octahedra were applied: i) (for the natrolite phase) the distances between Si-O and Al-O were restrained to target values of 1.620 ± 0.001 Å and 1.750 ± 0.001 Å, respectively, and the O-O distances to 2.646 ± 0.005 Å for the Si-tetrahedra and 2.858 ± 0.005 Å for the Al-tetrahedra[9, 20], ii) (for the lawsonite phase) the distances between Si-O and O-O of the tetrahedra were restrained to 1.620 ± 0.001 Å and 2.645 ± 0.005 Å, respectively, and the Al-O and O-O distances to 1.930 ± 0.001 and 2.729 ± 0.001 Å for the octahedra.[7, 8] The distribution of the non-framework species in the pores was established using successive difference Fourier syntheses. In the final stages of the refinements, the weights of the soft-restraints were gradually reduced, which did not lead to any significant changes of the inter-atomic distances. The final convergence of the refinement was achieved by varying simultaneously all background and profile parameters, scale factor, lattice constants, 2θ zero, and the atomic positional, fractional, and displacement parameters.

Fourier transform infrared spectroscopy measurements

FTIR spectra of the samples were obtained using an attenuated total reflectance (ATR)–FTIR spectrometer of the type Bruker Vertex 70v in conjunction with a FTIR Bruker Hyperion 2000 microscopy attachment equipped with the 4× viewing objective and 15×IR objective. The standard detector, a 250 µm liquid nitrogen cooled, mid-band mercury–cadmium–telluride (MCT) detector (ATR objective GMBH, Germany) with preamplifier, with the range of the IR spectrum from 4000 to 600 cm^{-1} was used. The spectra were measured with 4 cm^{-1} resolution and 64 scans condition.

High-angle Annular Dark-Field Scanning Transmission Electron Microscopy (HAADF-STEM)

HAADF-STEM images were acquired on an aberration-corrected JEOL 2100 F using a CEOS corrector and a Fischione Model 3000 detector with a camera length such that the inner cut-off angle of the detector was 75 mrad. The scanning acquisition was synchronized to the 60 Hz AC electrical power to minimize 60 Hz noise in the images, and a pixel dwell time of 24 µs was used.

Acknowledgements

This work was supported by the Global Research Laboratory (NRF-2009-00408) and National Research Laboratory (NRF-2015R1A2A1A01007227) Programs of the Korean Ministry of Science, ICT and Planning (MSIP). Experiments using X-ray synchrotron radiation were supported by Stanford Synchrotron Radiation Lightsource (SSRL) at Stanford University and Pohang Accelerator Laboratory (PAL) at POSTECH in Korea. We thank A. Metha, V. Borzenets, and R. Marks for the support at beamline BL10-2 at SSRL and H.-H. Lee and T. Jeon at beamline 9A at PAL.

Notes and references

1 D. L. Bish and D. W. Ming, *Natural Zeolites : occurrence, properties, applications*, Mineralogical Society of America, Washington DC, 2001.
2 J. Im, D. Seoung, S. Y. Lee, D. A. Blom, T. Vogt, C.-C. Kao and Y. Lee, *Environ. Sci. Technol.*, 2014, **49**, 513-519.
3 A. O. W. Leung, N. S. Duzgoren-Aydin, K. C. Cheung and M. H. Wong, *Environ. Sci. Technol.*, 2008, **42**, 2674-2680.
4 A. Hanson, *Industrial Materials*, 1995, 40-55.
5 U. Nadeem, *Eur. Chem. Bull.*, 2014, **3**, 495-501.
6 D. Seoung, Y. Lee, C. C. Kao, T. Vogt and Y. Lee, *Chem. Mater.*, 2015, **27**, 3874-3880.
7 W. H. Baur, *Am. Mineral.*, 1978, **63**, 311-315.
8 G. Dörsam, A. Liebscher, B. Wunder, G. Franz and M. Gottschalk, *N. Jb. Miner. Abh.*, 2011, **188**, 99-110.
9 Y. Lee, D. Seoung and Y. Lee, *Am. Mineral.*, 2011, **96**, 1718-1724.
10 Y. Lee, J. A. Hriljac, J. B. Parise and T. Vogt, *Am. Mineral.*, 2005, **90**, 252-257.
11 D. Seoung, Y. Lee, C. C. Kao, T. Vogt and Y. Lee, *Chem. Eur. J.*, 2013, **19**, 10876-10883.
12 I. D. Brown, *Chem. Rev.*, 2009, **109**, 6858-6919.
13 A. Le Cleac'h and P. Gillet, *Eur. J. Mineral.*, 1990, **2**, 43-53.
14 E. Libowitzky and G. R. Rossman, *Am. Mineral.*, 1996, **81**, 1080-1091.
15 H. P. Scott and Q. Williams, *Phys. Chem. Minerals*, 1999, **26**, 437-445.
16 D. Liu, W. Lei, Z. Liu and Y. Lee, *J. Phys. Chem. C*, 2010, **114**, 18819-18824.
17 Y. Lee, D. Liu, Z. Liu, D. Seoung and Y. Lee, *Am. Mineral.*, 2012, **97**, 419-424.
18 D. Liu, X. Chen, Y. Ma, Z. Liu, T. Vogt and Y. Lee, *Chempluschem*, 2014, **79**, 1096-1102.
19 Y. Lee, Y. Lee and D. Seoung, *Am. Mineral.*, 2010, **95**, 1636-1641.
20 Y. Lee, D. Seoung, D. Liu, M. B. Park, S. B. Hong, H. Chen, J. Bai, C. C. Kao, T. Vogt and Y. Lee, *Am Mineral*, 2011, **96**, 393-401.
21 A. P. Hammersley, S. O. Svensson, M. Hanfland, A. N. Fitch and D. Häusermann, *High Pressure Res.*, 1996, **14**, 235-248.
22 H. O. K. Mao and R. J. Hemley, *Philos. Trans. A Math. Phys. Eng. Sci.*, 1996, **354**, 1315-1332.
23 S. Klotz, J. C. Chervin, P. Munsch and G. Le Marchand, *J. Phys. D Appl. Phys.*, 2009, **42**.
24 P. M. Bell and H. K. Mao, *Absolute pressure measurements and their comparison with the ruby ß uorescence (R1) pressure scale to 1.5 Mbar*, Carnegie Institution, Carnegie Institution of Washington Year Book, 1979.

25 H. K. Mao, J. Xu and P. M. Bell, J. Geophys. Res.-Solid, 1986, **91**, 4673-4676.
26 A. C. Larson and R. B. V. Dreele, *GSAS-General Structure Analysis System*, Los Alamos National Laboratory, 1986.
27 H. M. Rietveld, *J. Appl. Crystallogr.*, 1969, **2**, 65.

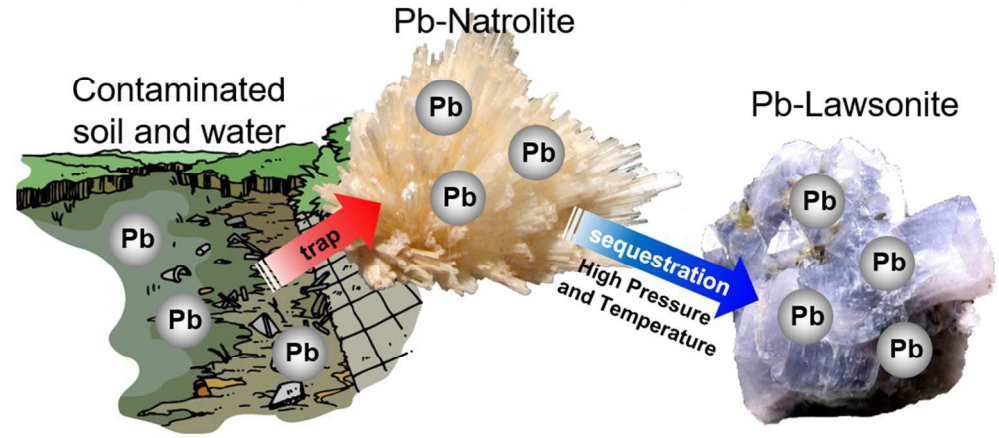

184x85mm (150 x 150 DPI)